Radiology: Imaging Cancer

REVIEW

Development of Multispectral Optoacoustic Tomography as a Clinically Translatable Modality for Cancer Imaging

*William M. MacCuaig, BS** • *Meredith A. Jones, BS** • *Oshaani Abeyakoon, MD, PhD* • *Lacey R. McNally, PhD*

From the Stephenson Cancer Center (W.M.M., M.A.J., L.R.M.) and Department of Surgery (L.R.M.), University of Oklahoma, 755 Research Parkway, 1 Medical Center Blvd, Oklahoma City, OK 73104; Department of Biomedical Engineering, University of Oklahoma, Norman, Okla (W.M.M., M.A.J., L.R.M.); and Department of Interventional Radiology, University College Hospital London, London, England (O.A.). Received May 27, 2020; revision requested June 17; revision received August 12; accepted August 19. **Address correspondence to** L.R.M. (e-mail: *lacey_mcnally@hotmail.com*).

*W.M.M. and M.A.J. contributed equally to this work.

Conflicts of interest are listed at the end of this article.

Radiology: Imaging Cancer 2020; 2(6):e200066 • https://doi.org/10.1148/rycan.2020200066 • Content code: OI

The use of optoacoustic imaging takes advantage of the photoacoustic effect to generate high-contrast, high-resolution medical images at penetration depths of up to 5 cm. Multispectral optoacoustic tomography (MSOT) is a type of optoacoustic imaging system that has seen promising preclinical success with a recent emergence into the clinic. Multiwavelength illumination of tissue allows for the mapping of multiple chromophores, which are generated endogenously or exogenously. However, translation of MSOT to the clinic is still in its preliminary stages. For successful translation, MSOT requires refinement of probes and data-acquisition systems to tailor to the human body, along with more intuitive, real-time visualization settings. The possibilities of optoacoustic imaging, namely MSOT, in the clinic are reviewed here.

Optoacoustic imaging is an emerging imaging method that has recently gained popularity as a clinically translatable technique. Optoacoustic imaging uses the photoacoustic effect, which is the generation of mechanical pressure waves as a result of light absorption of chromophores and subsequent thermoelastic contractions (Fig 1). Advantageous to conventional and optical imaging techniques, optoacoustic imaging uses near-infrared (NIR) light, which is highly transparent to biologic tissue as an excitation source. The high-transparency characteristics of NIR light mitigate the issue of photon scatter in tissue and therefore allow for increased-depth penetration into tissue with reduced sacrifice to resolution (1,2). In essence, high spatiotemporal and spectral resolution from light-based illumination imaging is merged with excellent depth penetration of US imaging to result in a clinically relevant tool for noninvasive imaging (3,4).

It is important to note the tradeoff between resolution and imaging depth, as optoacoustic techniques range from having macroscopic purposes (optoacoustic and photoacoustic CT) to microscopic purposes (optoacoustic microscopy) (5). Although optoacoustic microscopy is better suited for high-resolution imaging, lack of depth penetration limits applications to topical imaging. As an example, two major types of optoacoustic microscopy are optical-resolution photoacoustic microscopy and acoustic-resolution photoacoustic microscopy. Both optical- and acoustic-resolution photoacoustic microscopy use narrow field–illumination lasers with high-frequency transducers that must be mechanically translated to acquire three-dimensional (3D) images. A systematic distinction between acoustic-resolution and optical-resolution photoacoustic microscopy is in the illumination beam. Acoustic-resolution photoacoustic microscopy uses a laser that is either loosely focused or not focused with a focused-detection transducer, whereas optical-resolution photoacoustic microscopy uses a tightly focused incident beam. The different beams produce differences in the lateral spatial resolution, in which optical-resolution photoacoustic microscopy is better than acoustic-resolution photoacoustic microscopy (6). Although the clinical applications of optoacoustic microscopy are heavily limited by a penetration depth of a few millimeters, they are advantageous in that only the small focal region must be illuminated, allowing for the use of inexpensive low-powered lasers (7).

Optoacoustic tomography can image at depths up to 5 cm, allowing for noninvasive organ imaging in a clinical setting. Typically, optoacoustic tomographic systems use large-field illumination and capture generated ultrasonic waves with a two-dimensional or 3D array of transducers. Substantial improvements in optoacoustic detection systems have allowed for real-time image visualization, a valuable feature in the clinic. Further, optoacoustic tomographic systems have been equipped with multiwavelength illumination capabilities, which allow for separation of the complex signal into additive subcomponents, otherwise known as spectral unmixing (5). Addition of multiwavelength illumination to optoacoustic tomography creates a powerful tool that allows for a noninvasive and spectrally enhanced clinical method of tracking multiple agents within the body, known as multispectral optoacoustic tomography (MSOT) (5,8). Several companies have developed commercially available optoacoustic tomographic systems for medical imaging (Table 1). Most often, optoacoustic tomographic imaging systems are coupled with US imaging capabilities to provide a complete anatomic and/or optoacoustic signal map of the target tissue (Fig 2) (4,9,10).

Akin to other imaging techniques, MSOT and other optoacoustic imaging technologies employ reporter agents,

Abbreviations

ICG = indocyanine green, MSOT = multispectral optoacoustic tomography, NIR = near infrared, OPO = optical parametric oscillating, 3D = three-dimensional

Summary

Multispectral optoacoustic tomography is a rapidly emerging modality with recognized potential in the context of clinical adaptation for the purpose of imaging cancer.

Essentials

- Multispectral optoacoustic tomography (MSOT) is an optoacoustic imaging modality that mitigates issues such as low sensitivity, potential bodily risks, and high cost, which are inherent to conventional imaging techniques.
- Recently, a few clinical applications of MSOT have emerged, such as for breast, prostate, gynecologic, and dermatologic cancers.
- Spectral unmixing algorithms allow for detection of multiple chromophores, which can be visualized separately in real time or merged offline.

whether endogenous to the body or exogenous, to enhance contrast for identification of disease. Most diseases tend to result in overexpression or alteration of various molecules in the body, some of which are optoacoustic by nature and are therefore detectable directly by using MSOT (8,11,12). The use of these endogenous agents eliminates the need for unnecessary risk associated with introduction of a drug into the body, while still providing structural and functional information. However, endogenous agents are often weak reporting agents in terms of specificity and intensity. To this end, a wide range of exogenous agents have been under development to mitigate this issue of sensitivity and be used in detection and tracking of the progression of various diseases. Some of these exogenous agents include NIR organic dyes and nanostructures with modified surfaces (12,13). Although standard techniques have proven adequate, there is much room for growth when considering reconstruction, visualization, and quantification methods in MSOT.

The potential value of optoacoustic imaging, namely MSOT, in the clinic has been recognized, but successful clinical translation is currently in preliminary stages (14). Indeed, with development of contrast agents and technological advances, in terms of excitation, detection, and computation, the clinical relevance of MSOT has substantially increased. This article overviews optoacoustic imaging configurations, visualization, endogenous and exogenous contrast agents, and emerging applications in a clinical setting.

System Configurations

There are many different clinical optoacoustic tomographic imaging platforms, each consisting of a laser, a transducer, and a data-acquisition and image-processing system. The incident laser delivers NIR light in nanosecond pulses to illuminate the entire region of interest within tissue. Low-powered lasers (approximately 6 W) allow for a high pulse-repetition frequency, yielding improved signal-to-noise ratios, assuming no misregistration as a result of motion. These lasers are often smaller and less expensive than high-powered lasers but require more averages to increase the signal-to-noise ratio (15). MSOT uses a higher-powered (1.25-MW) pulsed, optical parametric oscillating, neodymium-doped yttrium–aluminum–garnet solid-state laser to excite the tissue.

Once an optoacoustic signal is generated by the tissue, it will propagate outward to be detected by low-frequency transducers. In turn, these transducers convert the mechanical optoacoustic signal to an electrical signal for subsequent image processing. Low-frequency transducers are used because of the capability to detect strong, low-frequency optoacoustic signals. These low-frequency signals are subject to less acoustic attenuation than high-frequency signals, allowing for deeper imaging (6). The transducers used depend on system configuration, but frequently, one-dimensional or two-dimensional linear-array transducer systems are found to be advantageous for optoacoustic imaging. Although integration of optoacoustic lasers into existing US systems seems attractive, the transducers used in clinical US machines are typically not broadband enough to handle optoacoustic signals (16,17).

A linear-array transducer can have either a planar or a curved detection geometry, optimized for imaging of superficial targets such as the skin or microvasculature. The feasibility of using linear-array transducers in the clinic is limited by a small field of view, poor image quality, and frequent artifact introduction (18). Curved linear-array detectors are typically seen as arc-shaped detectors with rotational stages for image acquisition in multiple positions. The ability to scan along the axial direction to create 3D images has yielded better spatial resolution and a higher sensitivity than has been yielded by planar linear-array detectors (18,20). The Vevo LAZR (VisualSonics, Toronto, Ontario, Canada) is a commercially available small-animal imaging system that uses a curved linear-array transducer with a stepper motor to create 3D images (21).

Hemispheric transducer arrays, or circular-array transducers, are arranged in a bowl-like structure with an opening for laser excitation. Clinically, these have been used in optoacoustic mammography to acquire complete 3D volumetric information (22). This configuration and other 3D configurations are advantageous in that each has a wide field of view that provides high-quality images, as there is complete information for reconstruction. Although these systems produce quality images, limitations stem from the need to encompass the entire region of interest, a task that is not always feasible in the clinic. The Nexus 128 (Endra, Ann Arbor, Mich) is a commercially available small-animal optoacoustic imaging system with 128 transducers arranged in a hemispheric configuration allowing for 3D reconstructions (21). Deán-Ben and Razansky have developed a handheld hemispheric transducer probe to acquire volumetric MSOT images from a small field of view in real time (23). Volumetric MSOT has the ability to obtain molecular, functional, and anatomic information in real time, a feature not present in the majority of current imaging modalities.

Image Processing and Visualization

MSOT uses multiple wavelengths to acquire optoacoustic images, allowing for the identification of multiple distinct

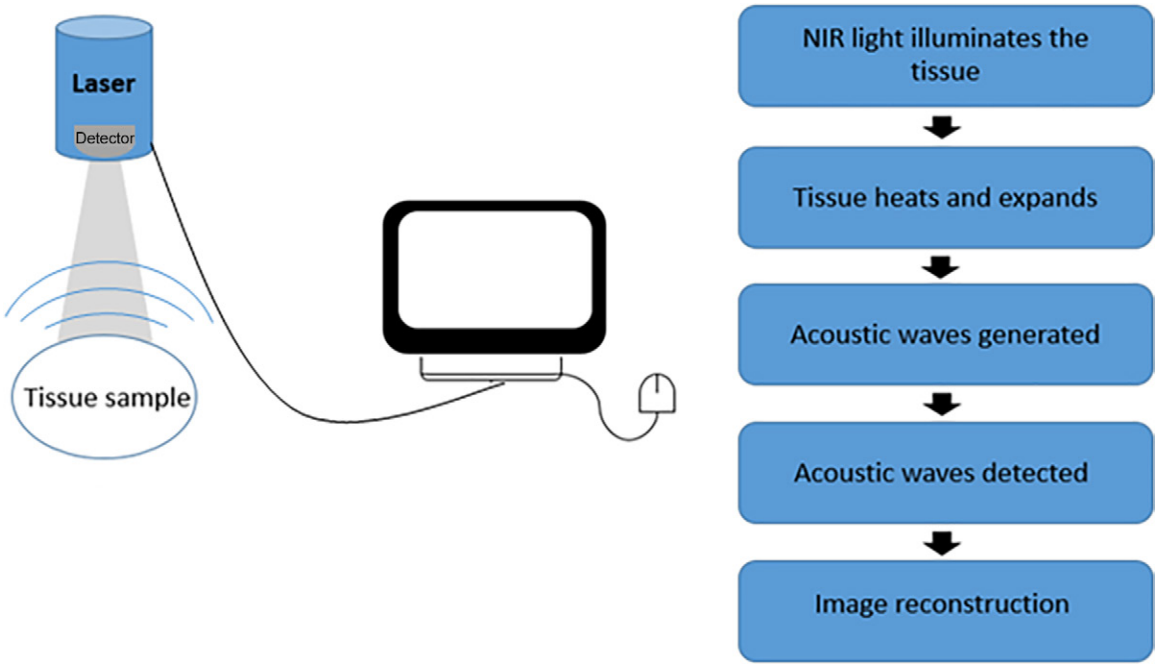

Figure 1: Schematic of process of optoacoustic signal generation through image reconstruction. NIR = near infrared.

Table 1: Available Optoacoustic Imaging Devices and Characteristics

Parameter	MSOT Acuity*	Imagio*	Vevo LAZR-X
Manufacturer	iThera Medical	Seno Medical	VisualSonics
Image acquisition	Arc-shaped detector array, 256 elements, 4 MHz	Linear detector array, 128 elements, 5 MHz	Linear detector array, 256 elements, 9–70 MHz
Penetration depth	Up to 50 mm	Up to 20 mm	Up to 30 mm
Laser wavelength	660–1300 nm	757 nm and 1064 nm	680–970 nm, 1200–2000 nm
Wavelength tuning speed	<10 msec	NA (only two wavelengths)	<1 sec
Resolution	<400 mm	Not documented	30 mm
Sensitivity	<100 nM for dyes in phantoms	Not documented	<500 nM for dyes in phantoms
US	Integrated US (Acuity-Echo)	Integrated US	Integrated advanced US
Spectral processing	Real-time spectral unmixing for several contrast agents	Ratio comparison of two wavelengths for hemoglobin	Offline spectral unmixing for several contrast agents

Note.—MSOT = multispectral optoacoustic tomography, NA = not applicable.
* Conformité Européenne–marked systems

chromophores based on unique spectral identifiers (8). If the image needs to be reconstructed in real time, a back projection reconstruction can be used. Although sufficient, back projection places a higher emphasis on high-frequency signals and produces negative values in the images (24). MSOT software allows the user to modify the bandpass filter to adjust the low- and high-frequency cutoffs and remove the negative values before back projection reconstruction. A more accurate reconstruction algorithm is a model-based approach. This approach factors in the geometry of the transducer, yielding a more accurate image, but this is at the cost of computational performance time. Model-based reconstructions are favorable and frequently used to reconstruct offline (24).

After successful reconstruction, the spectral shapes of these chromophores must be unmixed from each other and the background to positively identify respective origins. The process of spectral unmixing requires subpixel detection in that the signal produced from each individual pixel can be a composite signal from one or more chromophores in different concentrations. High heterogeneity of human tissue also has a substantial effect on the acoustic properties of the tissue, resulting in wavelength- and position-dependent optical fluence problems that affect the spectral signature produced. This phenomenon is commonly termed *spectral coloring* (25,26). The nonuniformity of human tissue poses a challenge for characterizing the optical properties of tissues; however, complex nonlinear mathematic formulations can be used to account for the spectral coloring (25,27).

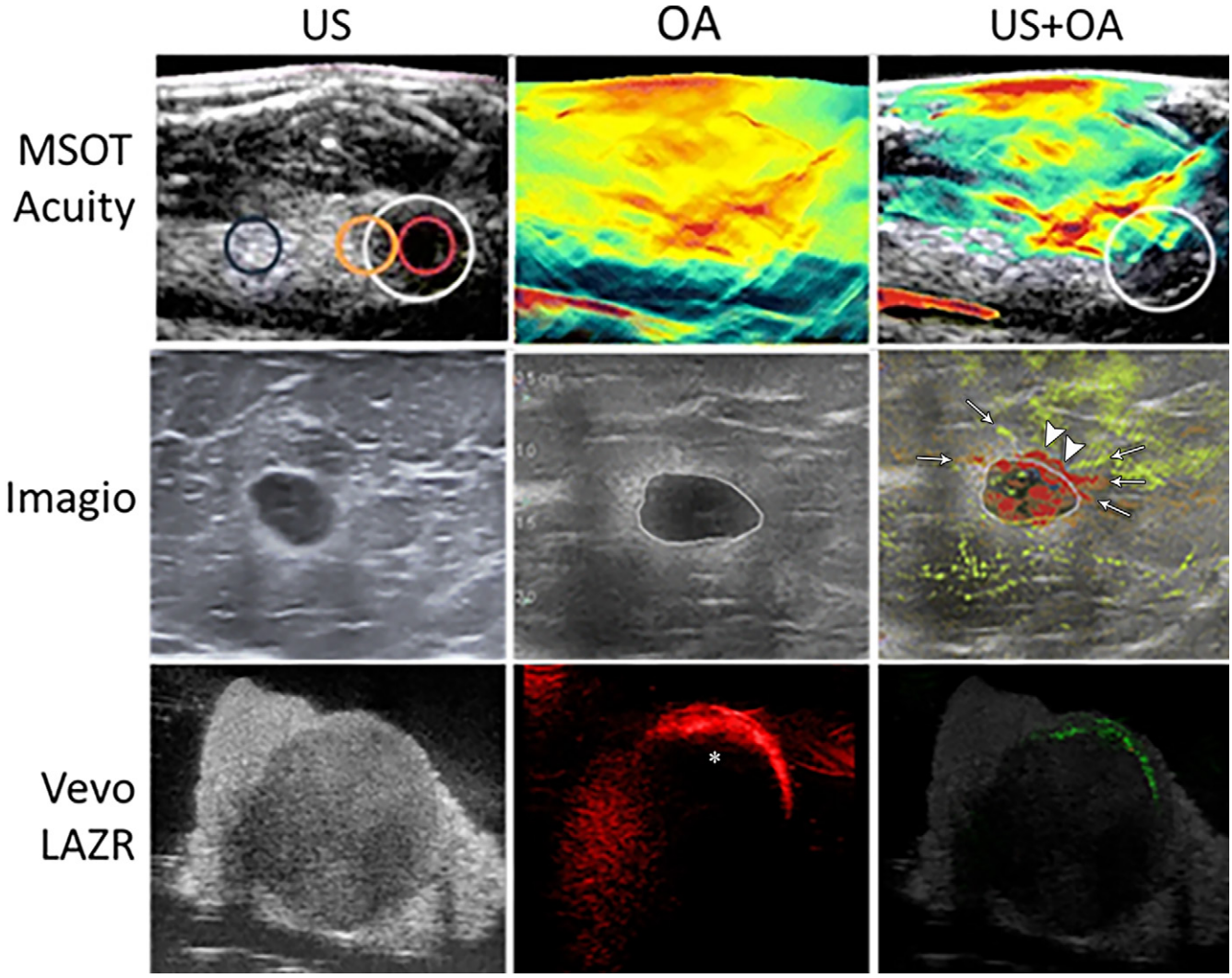

Figure 2: Multispectral optoacoustic tomographic (MSOT) images from different commercially available optoacoustic (OA) medical imaging systems. Images were acquired noninvasively from patients with breast cancer (MSOT Acuity [iThera Medical] and Imagio [Seno Medical]) or from excised lymph nodes in patients with melanoma (Vevo LAZR [VisualSonics]). Each set of images exhibits US imaging, OA imaging, and the overlay of the two modalities. Adapted, with permission, from references 4 (MSOT Acuity), 9 (Imagio), and 10 (Vevo LAZR).

When using MSOT in vivo, a linear regression is used to unmix the spectral signatures in real time. To use a linear-regression unmixing method, the spectra of interest must be predefined, usually as oxyhemoglobin, deoxyhemoglobin, and another agent of interest. Although linear unmixing models are most commonly used, these models assume that wavelength- and depth-dependent fluence issues are uniform and therefore can be neglected (28). Many different unmixing algorithms have been successfully developed to obtain information of interest, but there is no reference standard. The unmixing algorithms include statistical detection methods such as adaptive match filters, adaptive cosine estimators, principle component analysis, and independent component analysis. These statistical methods model the background as a multivariate distribution, in which statistical outliers are then defined as locations of positive targets (25,26). Modeling the background as a statistical distribution handles spectral coloring by accounting for spectral fluctuations. Statistical methods are successful for small, spatially constrained targets, such as solid tumors or tissue metastases, but would fail in cancers in which the target is spread throughout the blood or background tissue. Principal and independent component analyses are unique in that they can be used blindly, with no prior knowledge of the target spectra. Although seemingly advantageous, these blind methods introduce uncertainty and are often not reproducible (25).

After successful unmixing, the image can be visualized where signal from each optoacoustic agent is layered on a grayscale background image. The wavelength of the background image can be chosen on the basis of the experimental needs. Choosing a wavelength around 900 nm for the background image will highlight anatomic features while minimizing background contributions from the strongly emitting chromophores, oxyhemoglobin, and deoxyhemoglobin. The background image can be modified offline at any point in the image processing. Preclinically, it is possible to visualize multiple chromophores on the same background image in real time. However, clinical MSOT imaging in real time requires

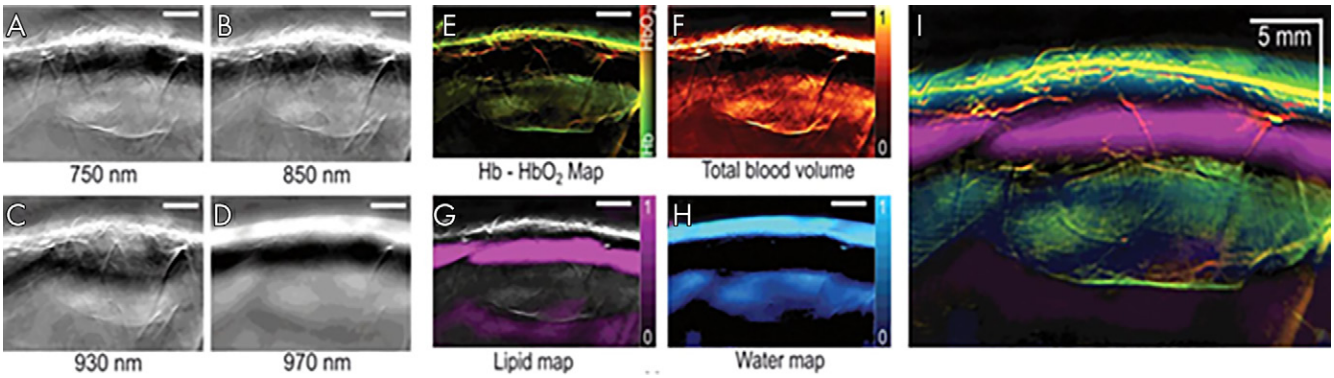

Figure 3: *A–D,* Multispectral optoacoustic tomographic (MSOT) images of human breast reconstructed online using a delay-and-sum method. *E–H,* The same MSOT images reconstructed offline using a model-based method followed by linear unmixing. *I,* Merged image of all four absorbers unmixed and visualized in images *E–H*. Adapted, with permission, from reference 8. Hb = deoxyhemoglobin, HbO_2 = oxyhemoglobin.

each agent of interest to be in a different panel. Offline, the different agents can be merged and layered to visualize their interactions (Fig 3) (8).

Contrast Agents

Endogenous Agents

Endogenous optoacoustic agents are attractive because their use eliminates the need for introduction of any additional materials into the body. However, the application of endogenous agents is small; specificity regarding target molecular processes is often disrupted by the abundance and nonspecificity of the agent. Blood proves to be the strongest endogenously available optoacoustic contrast agent because of the absorption profile of hemoglobin (11). Most notably, oxyhemoglobin portrays a different absorption profile than deoxyhemoglobin, resulting in the two molecules exhibiting unique spectral signatures (Fig 4, *A*) (29,30). Differentiation of spectral shape allows for visualization and determination of telling features, potentially providing information on the location of necrotic, hypoxic, or angiogenic areas (31). This information is particularly relevant in the context of measuring tumor response to therapies, and these locations can also be used as biomarkers (32,33). Such preclinical studies provide potential evidence for future human applications. Spectra of both oxyhemoglobin and deoxyhemoglobin reside within NIR window 1, defined as the space between 650 and 950 nm. Although melanin provides a strong optoacoustic signal, high concentrations coupled with nonspecific biodistribution could potentially hinder the ability to resolve other optoacoustic agents (34). However, incorporation of melanin into other exogenous contrast agents may serve to mitigate the issue of nonspecific distribution. Melanin falls into both NIR-absorbing windows, exhibiting high absorbance level between 650 and 1350 nm. Other endogenous optical absorbing agents have been detected in tissue, including water, lipids, bilirubin, cytochromes, elastin, and collagen, as well as DNA and RNA (13). Because all of these endogenous agents have unique NIR absorbance profiles, the issue of nonspecific distribution within the body limits efficacious use as a targetable agent for preclinical research and subsequent translation.

Exogenous Agents

Introduction of exogenous optoacoustic agents circumvents the issue of nonspecificity associated with endogenous agents. As previously mentioned, in many diseases, there are unique molecular signatures that could be exploited for tracking of related cellular processes (eg, extracellular expression of epidermal growth factor receptor on cancer cells). Further, absorption profiles of these exogenous agents are often tunable; slight alterations in structure or synthesis procedure may yield unique distinction in absorption profiles, allowing for improved spectral unmixing of multiple agents. In contrast to endogenous materials, use of exogenous contrast agents creates a dose-to-signal tradeoff, raising concerns of toxicity (13).

Organic dyes.—Clinically approved organic dyes, including indocyanine green (ICG) and methylene blue have been shown to generate optoacoustic signal in addition to the more commonly addressed feature of generating fluorescence signal (35) (Fig 4, *B*). Particularly, ICG rapidly binds large-sized albumin, creating an impermeable probe for detection with optoacoustic modalities. Isosulfane blue is another example of an organic dye used for photoacoustic imaging (36). In addition, a variety of fluorescence molecules have shown the potential for generating optoacoustic signal detectable with modalities such as MSOT. These include cyanine dyes and NIR proteins such as Cy-series (37) and the iRFP-series (38) of agents. An example of an NIR dye is IR800CW (39), which is currently in phase II trials for fluorescence imaging and has shown optoacoustic signal generation with associated imaging targets (40). Recently, the potential for the use of squaraine dyes in optoacoustic applications has been summarized, with the summary including how structural characteristics are thought to affect absorption spectra (41). Synthesized organic dyes are most often used for perfusion imaging when used as single-element contrast agents, but incorporation into other technologies provides improvements to photostability, clearance, and specificity by active targeting for use as a molecular probe (42).

Nanoparticles.—Gold nanoparticles have been among the most-studied metal-based optoacoustic contrast agents, as the

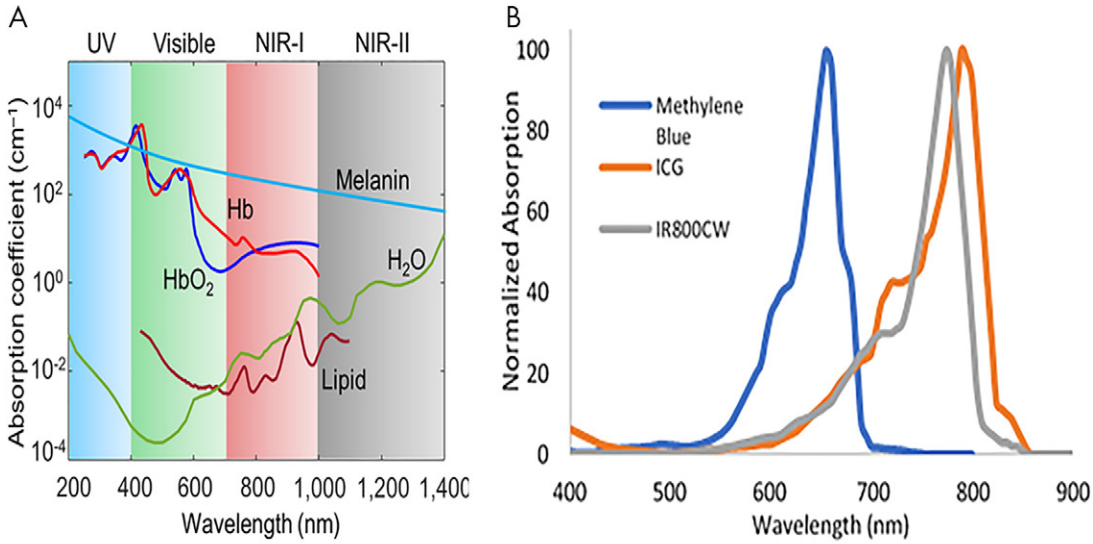

C

Material	Absorbance Range (nm)	Aspect controlling peak absorbance	Reference
Gold nanorods	700-900	Aspect Ratio	Zeiderman et. al. (1)
Gold nanospheres	500-650	Size	He et. al. (2)
Iron-oxide	300-500	Method of synthesis	Hashem et. al. (3)
Silver	400-600	Size	Paramelle et. al (8)
Carbon Nanotubes	300-1300	Chirality, Preparation time, Number of Walls	Pfohl et. al. (9), Cheng et. al. (11)

Figure 4: Absorption profiles of select, *A*, endogenously generated contrast agents and, *B*, organic-dye contrast agents. *C*, Outline of nanoparticles used for optoacoustic contrast generation. Adapted, with permission, from reference 30. Reference citations in *C* correspond to the reference list in the original publication. ICG = indocyanine green, NIR = near infrared, UV = ultraviolet.

physical shape of these particles provides an opportunity to craft a highly distinguishable absorption spectrum (43) (Fig 4, *C*). Further, gold naturally provides high absorption of NIR light, resulting in a strong optoacoustic signal. Because of ease of synthesis and established methods, gold nanoparticles have been studied in their conventional spheric conformation, as well as in the shape of rods, shells, and other unique conformations, mostly in the context of tumor imaging (44,45). However, the strong and distinguishable signal is accompanied by toxicity, namely induction of reactive oxygen species and accumulation in the liver and spleen (46). Surface modifications of these particles are essential when considering the goal of clinical translation, as these modifications could partially mitigate issues of toxicity but may come at the expense of reduced optoacoustic signals. Other types of metal-based nanoparticles have shown optoacoustic activity, such as silver and iron oxide (47,48). Often, absorption profiles of nanoparticles are tunable according to structural characteristics (Fig 4, *C*). In addition to metal-based particles, carbon nanotubes are another form of specialized optoacoustic nanoparticle, with sizes less than 5 nm, that relies heavily on the aforementioned surface modifications (49,50). With the core particle–synthesis procedure of metal-based nanoparticles having been well established, recent focus in this area has concerned the development of activatable optoacoustic agents and surface modifications. These modifications aim to relieve toxicity, incorporate active targeting for specificity, or enable inclusion of other contrast agents within the particles for controlled delivery (12,13).

Clinical MSOT Applications

Breast Imaging

Breast cancer is the leading cause of cancer-related deaths among women. In 2020, it is predicted that 279 100 new cases of breast cancer will be diagnosed in the United States, with 42 690 of those cases resulting in death (51). As with many cancers, imaging is used for the screening, diagnosis, and monitoring of breast cancer. Traditionally, x-ray mammography is used for population-based screening. For young patients presenting with symptoms of breast disease, US is the modality of choice. In women over the age of 40, mammography and US are used as the first-line modalities. Both modalities have limitations (52,53) that result in false-positive findings and, in the case of mammography, decreased sensitivity with increasing breast density. Both techniques detect morphologic detail (54). Dynamic contrast agent–enhanced imaging overcomes these

challenges with high sensitivity and specificity (54); however, it is limited by high expense and low availability. A low-cost technique to improve the sensitivity and specificity of mammography and US would be a welcomed addition to the breast clinic.

The breast is a fatty superficial organ suitable for optoacoustic imaging; relatively low-depth penetration is required and results in high-resolution information. Clinical prototypes to image the human breast have handheld or arc-shaped probes. Over a period of approximately 10 years, the technology has evolved from attempting to visualize breast cancer to possessing the ability to differentiate benign from malignant lesions (55). In 2016, Deán-Ben et al developed a volumetric handheld optoacoustic device for real-time in vivo imaging of the vasculature in dense breast tissue (56). An optical parametric oscillating Q-switched laser emits 10-nsec pulses at wavelengths of 730, 760, 800, and 850 nm at the target tissue. Introduction of optical parametric oscillating lasers to optoacoustic imaging allows for fast-pulse illumination, which enables rapid visualization of multiple chromophores. A handheld probe with a semispheric 256-element array is used for acoustic wave detection. After reconstruction and unmixing, distribution maps of oxyhemoglobin, deoxyhemoglobin, and melanin were created and analyzed to identify highly vascularized areas. These areas of abnormal vasculature are indicators of angiogenesis, a hallmark of cancer and a widely accepted mark of solid tumors (31).

Toi et al used a handheld volumetric probe system, photoacoustic mammography with a hemispherical-shaped detector array, to visualize changes in the oxygenation status of blood vessels (arteries and veins) before and after chemotherapy with taxane (22) (Table 2) (1,3,8–10,19,22,56–69). An increase in visualization of blood vessels inside the tumor after therapy was realized, even though there was no change in the tumor size detected by using US. It is unclear whether this is a result of effective chemotherapy or just a morphologic change in the tumor microenvironment. This normalization of the tumor vasculature has been speculated to be an anticancer mechanism, but there is still uncertainty as to what was occurring (22). In a 2017 pilot study, Diot et al used fast-MSOT at 28 wavelengths between 700 and 970 nm to image angiogenic biomarkers of breast cancer, as well as the fat and water compositions of the tissue, to gain a better understanding of the difference between malignant and nonmalignant tissue (8) (Fig 3). The multispectral study allowed for increased visualization of the breast tissue, enabling extraction of more functional, molecular, and anatomic information. This can be immensely useful for clinical applications such as therapy planning and monitoring or intraoperative use of MSOT for clean surgical margins. Recently, Abeyakoon et al used the MSOT Acuity-Echo prototype from iThera Medical (Munich, Germany) to investigate vascular maps for potential to serve as a differentiating factor between benign and malignant breast disease (57). US combined with optoacoustic imaging resulted in extraction of detail related to the malignancy of disease (Fig 5) (57). By virtue of MSOT, higher diagnostic specificity was realized with no loss to sensitivity, strengthening the potential for translation of optoacoustic imaging into a clinical setting for breast imaging (57). The improved characterization of solid breast masses seen on images obtained through US with optoacoustic imaging was further described in two multicenter randomized controlled trials in the United States and the Netherlands (9,58). Quantification of the optoacoustic signal in the human breast has revealed changes that are in keeping with the physiologic changes of the normal menstrual cycle (70).

Advances in imaging have increased early detection of impalpable breast cancer. Often, the treatment of choice is breast-conserving surgery. Forty percent of patients who undergo breast-conserving surgery require a second surgery because of positive surgical margins (71). Development of intraoperative optical imaging to overcome this problem could enhance patient care (72). Development of molecular imaging probes to target specific breast-cancer receptors (estrogen receptor and human epidermal growth factor receptor 2 [HER2]) would enhance the molecular characterization (73), allowing for better treatment with hormonal therapy and trastuzumab. In addition, optoacoustic imaging coupled with standard grayscale US has differentiated HER2-positive and triple-negative breast cancers from luminal cancers (74). This further suggests the possible capability to differentiate HER2-positive breast cancers from triple-negative cancers, which exhibits high clinical significance as a noninvasive breast-cancer characterization technique (74).

Prostate Imaging

In 2020, an expected 191 000 new cases of prostate cancer will be diagnosed in the United States, with 17% of those cases resulting in a fatality (51). Prostate cancer is extremely common in elderly men and is characterized by slow growth, making it very likely to go untreated for decades. The presence of elevated prostate-specific antigen levels in the blood is a key indicator of prostate cancer, which prompts a transrectal US biopsy that yields a very low specificity because of blind needle insertion (75). MRI coupled with US before a prostate biopsy improves the specificity of the diagnosis but provides no functional information about the cancer (75). A clinical need for a noninvasive imaging modality that can yield a highly specific diagnosis along with information about the cancer on a molecular level is desirable.

Because transrectal US is a bedside imaging modality and is also inexpensive, it is ideal to incorporate optoacoustic systems into the pre-existing transrectal US systems. Recently, Kothapalli et al used a combination of transrectal US and optoacoustic imaging to develop a transrectal US and photoacoustic device to improve prostate cancer diagnosis (59). The transrectal US and photoacoustic system used a 64-element capacitive micromachined ultrasonic transducer array with a 5-MHz center frequency in the detection probe. A 5-nsec pulsed laser with 680- to 950-nm wavelength capabilities was used to illuminate the tissue from different angles. The images were displayed in real time at a rate of 10 frames/sec. ICG, a clinically approved optoacoustic dye, was used as an exogenous optoacoustic contrast agent because it binds to the plasma proteins in the vascular space (35). After multispectral processing of oxyhemoglobin, deoxyhemoglobin, and ICG, the vascularity of the prostate could be mapped to identify key prostate features (such as seminal vesicles, neurovascular bundles, the dorsal venous complex, and the prostate capsule) with higher spatial resolution than transrectal US.

Table 2: Clinical Applications of MSOT

Application	Type	Laser	Detector	Patients	Study
Breast imaging	MSOT	NIR laser at 28 wavelengths from 700 to 970 nm	256 elements, 5 MHz, arc transducer array	10 patients with breast cancer, 3 healthy volunteers	Diot et al (8)
Breast imaging	Handheld OA/US transducer	NIR laser at wavelengths of 757 and 1064 nm	Four conventional US diagnostic transducers	209 patients from 5 different sites	Menezes et al (9)
Breast imaging	OA microscopy	Q-switched alexandrite laser at 755 and 795 nm	512 elements, 2 MHz, hemispheric transducer array	30 patients with known breast tumors	Toi et al (22)
Breast imaging	Volumetric handheld probe	Q-switched OPO laser at 730, 760, 800, and 850 nm	256 elements, 4 MHz, spheric transducer array	2 women with dense fibroglandular breast tissue	Deán-Ben et al (56)
Breast imaging	MSOT+US	NIR laser at 800 nm	256 elements, 4 MHz, arc transducer array	94 patients between the ages of 24 and 88	Abeyakoon et al (57)
Breast imaging	Handheld OA/US transducer	NIR laser at wavelengths of 757 and 1064 nm	128 elements, 4- to 16-MHz, linear array	2105 patients from 16 different sites	Neuschler et al (58)
Prostate imaging	Transrectal US and photoacoustic device	Tunable pulsed laser, 680–950 nm	64 element, 5 MHz, CMUT linear array	20 patients with prostate cancer (10 with ICG, 10 without)	Kothapalli et al (59)
Gynecologic imaging	OA imaging	Q-switch Nd:YAG 532-nm laser	10-MHz focused transducer with 10-mm focal distance	30 ex vivo cervical tissue samples	Peng et al (60)
Gynecologic imaging	Co-registered transvaginal OA tomography/US	Pulsed Nd:YAG laser at 690–900 nm	128 elements, 6 MHz, endocavital US transducer	16 women	Nandy et al (61)
Gynecologic imaging	Fast-scanning, optical-resolution photoacoustic endoscopy	532-nm pulsed focused fiber laser	40 MHz custom-designed Focused US ring transducer	2 pregnant women	Qu et al (62)
Inflammatory bowel disease (Crohn disease)	MSOT	Pulsed Nd:YAG laser at 680–980 nm	64-element, 4-MHz and 256-element, 3-MHz, probes	108 patients	Knieling et al (3)
Inflammatory bowel disease (colitis)	MSOT	Pulsed Nd:YAG laser at 680–980 nm	64-element, 4-MHz and 256-element, 3-MHz probes	44 patients	Knieling et al (63)
Dermatologic imaging	MSOM	Flash lamp–pumped Nd:YAG OPO pulsed laser from 460 to 650 nm	54.2-MHz broadband spherically focused transducer	28-year-old healthy man	Schwarz et al (64)
Dermatologic imaging	Volumetric MSOT	690- to 900-nm tunable OPO pulsed laser	256 elements, 4 MHz, spheric transducer array	3 patients with skin lesions	Chuah et al (65)
Lymph node imaging	Vevo LAZR OA imaging	Pulsed laser, 680–970 nm	21 MHz, linear transducer array	12 lymph nodes ex vivo	Langhout et al (10)
Lymph node imaging	Handheld MSOT	ND:YAG tunable OPO laser from 680 to 980 nm	256 elements, 4 MHz, cylindrically focused detector array	20 patients with administered ICG	Stoffels et al (1)
Graves disease and thyroid cancer	Handheld MSOT	9-nsec pulsed laser from 700 to 950 nm	256 elements, 3 MHz, 40 × 40-mm field of view	18 patients	Roll et al (66)
Graves disease	Handheld MSOT	Pulsed laser, 700–970 nm	256 elements, 4 MHz, arc orientation	8 volunteers and 10 patients	Krönke et al (67)
Cardiovascular disease monitoring	Volumetric MSOT	Pulsed laser, 730–1064 nm	256 elements, spheric array	16 volunteers	Ivankovic et al (19)
Systemic sclerosis	Handheld US/MSOT	Pulsed Nd:YAG laser at 680–980 nm	256 elements, 4 MHz, linear array	8 volunteers and 7 patients	Masthoff et al (68)
Metabolic disease in adipose tissue	MSOT	Pulsed laser at 680–950 nm	256 elements, 5 MHz, cylindrically focused array	13 volunteers	Reber et al (69)

Note.—CMUT = capacitive micromachined ultrasonic transducer, ICG = indocyanine green, MSOM = multispectral OA mesoscopy, MSOT = multispectral optical tomography, Nd:YAG = neodymium-doped yttrium–aluminum–garnet, NIR = near infrared, OA = optoacoustic, OPO = optical parametric oscillating.

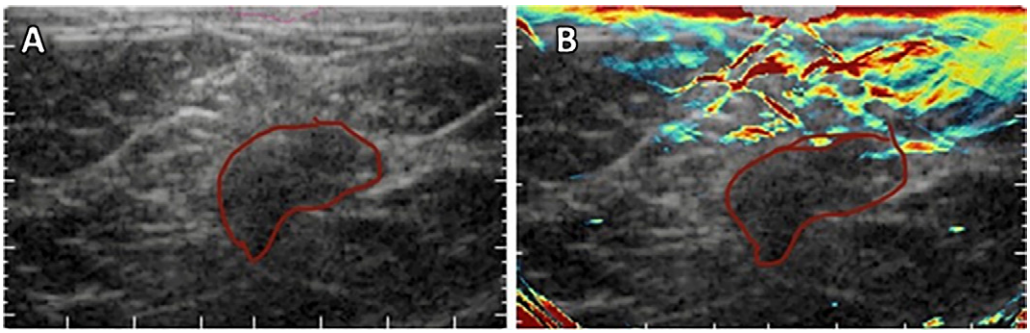

Figure 5: *A*, Anatomic US image and *B*, hybrid optoacoustic and US images of a grade 3 invasive ductal carcinoma. Hybrid imaging allowed visualization of the irregular cap of neoangiogenesis in relation to the hypoechoic irregular tumor mass. The tumor margin is outlined in red.

Gynecologic Imaging

In 2020, 6.2% of new cancer diagnoses are predicted to be gynecologic cancers, consisting of cervical, ovarian, vulvar, and vaginal cancer (51). Current diagnosis of cervical cancer is dependent on Papanicolaou test and pelvic examinations, with abnormal screening findings resulting in a cervical biopsy being performed, but both screening and biopsy have low specificity (60). For diagnosis and staging of ovarian cancer, which is the deadliest of the gynecologic cancers because of frequent late-stage diagnosis, the serum levels of the CA-125 tumor marker are typically assessed in combination with transvaginal US (12). Both methods have a very low sensitivity and specificity, indicating a pressing need for molecular targeting agents to decrease the false-positive and false-negative rates of gynecologic cancer screening.

A main obstacle with clinical translation of optoacoustic imaging for gynecologic cancers is the need to compact the optical detector into a transvaginal probe for internal scanning. Previously, 2.5-mm endoscopic optoacoustic probes have been reported and are the ideal size for use in the vaginal canal (76). In 2017, multispectral optoacoustic imaging enabled successful identification of 26 ovarian masses in patients with the use of a co-registered pulse-echo optoacoustic transvaginal probe (61). Anatomic locations of the masses were identified by using US, and the addition of multispectral optoacoustic imaging at four wavelengths (730, 780, 800, and 830 nm) allowed for quantification of blood oxygen saturation and hemoglobin concentrations such that benign and malignant masses could be differentiated (61).

A transvaginal, fast-scanning, optical-resolution optoacoustic endoscope was developed and used clinically to visualize the vascularity of the cervix (62). The addition of a laser capable of illumination at different wavelengths would enable identification of angiogenic and hypoxic environments, indicative of gynecologic cancers, using this device.

Gastrointestinal Imaging

A total of 333 680 new cases of gastrointestinal cancers are estimated to be diagnosed in 2020, with an estimated 167 790 deaths as a result (51). These cancers include esophageal, intestinal, and colorectal cancers, among others. Fusing optoacoustic imaging with traditional endoscopy or US techniques could have beneficial clinical applications in imaging of the gastrointestinal tract. The modalities currently used to evaluate the gastrointestinal tract include endoscopy, US, CT, and MRI. MSOT has been clinically assessed to determine whether its use could improve the noninvasive diagnosis of disease severity in inflammatory bowel disease using a transabdominal approach. Patients with inflammatory bowel disease have mucosal edema, causing inflammation that results in an increase in the amount of blood and water in intestinal tissues. Studies performed by Knieling et al suggest that the combination of clinical examination and US with MSOT can be helpful in the diagnosis and monitoring of inflammatory bowel disease (3,63). Inflammatory bowel disease is associated with an increased risk of malignancy; early diagnosis and monitoring may reduce risk and complications associated with malignancy.

Optoacoustic imaging fused with endoscopy improves the opportunity to characterize soft-tissue abnormalities with a luminal approach (3,63). Early detection of esophageal cancer and stratifying changes associated with Barrett esophagus has the potential to substantially improve the outcome of a malignancy, which typically has a delayed presentation and increased morbidity and mortality (77).

Dermatologic Imaging

An estimated 100 000 new cases of skin cancer within the United States are predicted for 2020 (51). Diagnosis of skin cancer begins with visual inspection, and then, if needed, a biopsy is performed. Optoacoustic imaging is an attractive option for the diagnosis and monitoring of skin cancers because of the noninvasive nature in comparison with traditional tissue biopsies. The thickness of the human skin is reported to be around 5 mm, making mesoscopic optoacoustic imaging systems relevant.

Use of 3D multispectral optoacoustic mesoscopy allows for the absorption mapping of oxyhemoglobin, deoxyhemoglobin, and melanin in the skin. Visualization of these endogenous chromophores can assist in the noninvasive diagnosis of cancer. Schwarz et al employed multispectral optoacoustic mesoscopy on the skin of a healthy man, using a flash lamp–pumped, neodymium-doped yttrium–aluminum–garnet, optical parametric oscillating 6-nsec pulsed laser at wavelengths from 460 to 650 nm to excite chromophores within the tissue. A broadband

spheric transducer with a central frequency of 54.2 MHz was used (64). In addition, photoacoustic imaging has been used to extract information such as lesion depth and vascular thickness in the context of port-wine stains, facilitating the selection of optimal parameters for laser therapy (78).

To our knowledge, the first use of clinical MSOT for skin tumors was performed in 2017 by Chuah et al. Their study analyzed unclassified skin lesions before they were biopsied and sent for histologic analysis. Real-time volumetric MSOT with a handheld probe was used to obtain 3D maps of oxyhemoglobin, deoxyhemoglobin, and melanin. From this information, tumor length, width, and depth could be determined, showing a noninvasive method to diagnosis skin tumors (65). MSOT imaging has also been used to image intact sentinel lymph nodes for the presence of melanin, indicating melanoma metastasis (10). Stoffels et al used MSOT with a clinically approved exogenous agent, ICG, to visualize the sentinel lymph nodes and determine the presence of metastasis. In this study, a total of 20 patients with peritumorally administered ICG were imaged using MSOT at five wavelengths: 700, 730, 760, 800, and 850 nm. They saw a 100% (41 of 41) sensitivity rate and a 48% (18 of 37) specificity rate in vivo for identifying metastasis-free lymph nodes on the basis of melanin detection (1). Following this, a 100% (189 of 189) sensitivity rate and a 62.3% (71 of 114) specificity rate were observed ex vivo. In 2019, Stoffels et al performed a multicenter study across four institutions. A total of 165 lymph nodes were collected from 83 patients. The concordance rate of ICG-labeled and technetium 99–marked detection of sentinel lymph node basins was 94.6% (106 of 112). Intraoperatively, 159 sentinel lymph nodes were detected using a NIR camera, and 165 were detected by using a gamma probe, resulting in a concordance rate of 96.4% (79). Routine use of MSOT in the clinic for diagnosis and management of melanomas will be beneficial (80). The ability to noninvasively identify malignancy of lymph nodes could reduce the need for unnecessary excisions and complications, while providing valuable tumor information for the subsequent surgical procedures (12).

Head and Neck Imaging

Differentiating among benign functional thyroid nodules, nonfunctional thyroid nodules, and malignancy is a challenge. Current imaging strategies include US with fine-needle aspiration. In 2016, Dima et al explored the feasibility of investigating the thyroid gland with MSOT. Healthy volunteers were imaged with MSOT, and produced images were comparable with Doppler US images (81). Roll et al used MSOT to image patients with Graves disease and compared findings with those from healthy volunteers. Their findings demonstrated that patients with Graves disease had thyroid lobes with higher deoxyhemoglobin and lower fat in comparison with patients with healthy tissue. Malignant thyroid nodules showed lower saturation of hemoglobin and lower fat content when compared with benign nodules (66). Further, Krönke et al showed that Graves disease and thyroid tumors demonstrated increases in oxyhemoglobin and deoxyhemoglobin, but with decreased oxygen saturation in relevant volumes (67).

Other Clinical Applications

Real-time MSOT imaging has shown promise for monitoring the human vasculature, which is particularly important for monitoring patient responses to cancer. MSOT can be used to discern differences of oxyhemoglobin and total hemoglobin in real time in the fingers of patients with diseased vasculature (68). Using MSOT to study metabolic process has been recently investigated as well. In this study, Reber et al were effectively able to use MSOT to distinguish brown adipose tissue from white adipose tissue and muscle on the basis of hemoglobin levels (69). Further, introduction of the patient into a cold environment induced heightened oxyhemoglobin levels, indicating an increase in metabolic activity (69). This study suggests use of MSOT for other metabolic diseases, such as diabetes, which is related to cancer through inflammation and cachexia. These clinical studies establish MSOT as a viable, noninvasive, bedside clinical modality for patients with cancers, inflammatory bowel diseases, and a variety of other conditions.

Limitations of Optoacoustic Imaging

The major limitation of optoacoustic imaging is depth. As light travels through tissue, it is predominantly absorbed and scattered. With increasing depth, the amount of light that penetrates to deeper tissues decreases exponentially, and thus the depth of imaging can vary between 5 mm and 5 cm. For example, a hemoglobin-rich kidney will only have a signal generated at the initial 5 mm of depth, or in a fatty breast, one may detect changes of neoangiogenesis 2.5 cm beneath the skin. Quantification of the optoacoustic signal at varying depths requires an algorithm to account for the absorption and scattering properties of the tissue. Obtaining precise numbers that accurately reflect the heterogeneity of biologic tissue is very complex. Success in clinical translation remains in creating scanners that are developed to answer specific clinical questions and in choosing superficial targets to assist in clinical decision-making. Furthermore, development and approval of exogenous contrast agents is required for wide adoption of optoacoustic imaging in the clinic. The small group of approved optoacoustic agents represents a substantial bottleneck for optoacoustic imaging techniques. Although these agents have been under focus recently, the approval process is rather lengthy, hindering adoption of optoacoustic imaging in the clinic. Although MSOT is Conformité Européenne–marked, it is not a Food and Drug Administration–approved instrument for clinical trials in the United States. However, there are opportunities to apply for investigational device exemption for use in clinical trials.

Conclusion

Although MSOT is still in a relatively new state as an imaging modality, emergence as a clinically translatable technique has ensued. Exploitation of the photoacoustic effect renders tissue scatter of generated signal irrelevant, allowing for high spatiotemporal resolution. Further, with NIR light–excitation beams, deeper overall tissue penetration and contrast than that obtained using

most optical imaging techniques can be achieved while still remaining noninvasive. Further, the use of advanced multispectral processing allows for tracking and quantifying multiple contrast agents. MSOT shows high potential to be used as a diagnostic tool in combinations with other modalities, or perhaps as an intraoperative real-time tool for many surgical applications, such as assessing tumor margins. However, particular sites within the body intrinsically limit the potential applications of MSOT. Bone is a strong optical absorber, which could limit the extent of application in situations such as noninvasive imaging of the brain. Further, the disparity in sound transmission of air and liquid is great; signals from areas such as the lung will produce less meaningful and detailed information about the functional state. The spectral coloring problem due to nonuniform attenuation of the excitation light creates an extremely complex reconstruction problem, making quantification difficult at depth. Last, the current lack of exogenous contrast agents limits MSOT applications to depending on endogenous agents such as blood. However, with rapid development of a plethora of optoacoustic dyes, some of the current limitations could be overcome in the years to come, further defining the position of MSOT in a clinical setting.

Disclosures of Conflicts of Interest: W.M.M. disclosed no relevant relationships. **M.A.J.** disclosed no relevant relationships. **O.A.** disclosed no relevant relationships. **L.R.M.** Activities related to the present article: institution received NIH grants (R01CA212350, R01EB020125, and R01CA205941). Activities not related to the present article: editorial board member of *Radiology: Imaging Cancer* (RSNA). Other relationships: disclosed no relevant relationships.

References

1. Stoffels I, Morscher S, Helfrich I, et al. Metastatic status of sentinel lymph nodes in melanoma determined noninvasively with multispectral optoacoustic imaging. Sci Transl Med 2015;7(317):317ra199.
2. Bhutiani N, Kimbrough CW, Burton NC, et al. Detection of microspheres in vivo using multispectral optoacoustic tomography. Biotech Histochem 2017;92(1):1–6.
3. Knieling F, Neufert C, Hartmann A, et al. Multispectral optoacoustic tomography for assessment of Crohn's disease activity. N Engl J Med 2017;376(13):1292–1294.
4. Becker A, Masthoff M, Claussen J, et al. Multispectral optoacoustic tomography of the human breast: characterisation of healthy tissue and malignant lesions using a hybrid ultrasound-optoacoustic approach. Eur Radiol 2018;28(2):602–609.
5. Ntziachristos V, Razansky D. Molecular imaging by means of multispectral optoacoustic tomography (MSOT). Chem Rev 2010;110(5):2783–2794.
6. Erfanzadeh M, Zhu Q. Photoacoustic imaging with low-cost sources: a review. Photoacoustics 2019;14:1–11.
7. Choi W, Park EY, Jeon S, Kim C. Clinical photoacoustic imaging platforms. Biomed Eng Lett 2018;8(2):139–155.
8. Diot G, Metz S, Noske A, et al. Multispectral optoacoustic tomography (MSOT) of human breast cancer. Clin Cancer Res 2017;23(22):6912–6922.
9. Menezes GLG, Pijnappel RM, Meeuwis C, et al. Downgrading of breast masses suspicious for cancer by using optoacoustic breast imaging. Radiology 2018;288(2):355–365.
10. Langhout GC, Grootendorst DJ, Nieweg OE, et al. Detection of melanoma metastases in resected human lymph nodes by noninvasive multispectral photoacoustic imaging. Int J Biomed Imaging 2014;2014:163652.
11. Li M, Tang Y, Yao J. Photoacoustic tomography of blood oxygenation: a mini review. Photoacoustics 2018;10:65–73.
12. McNally LR, Mezera M, Morgan DE, et al. Current and emerging clinical applications of multispectral optoacoustic tomography (MSOT) in oncology. Clin Cancer Res 2016;22(14):3432–3439.
13. Weber J, Beard PC, Bohndiek SE. Contrast agents for molecular photoacoustic imaging. Nat Methods 2016;13(8):639–650.
14. Zackrisson S, van de Ven SMWY, Gambhir SS. Light in and sound out: emerging translational strategies for photoacoustic imaging. Cancer Res 2014;74(4):979–1004.
15. Hariri A, Fatima A, Mohammadian N, et al. Development of low-cost photoacoustic imaging systems using very low-energy pulsed laser diodes. J Biomed Opt 2017;22(7):75001.
16. Beard P. Biomedical photoacoustic imaging. Interface Focus 2011;1(4):602–631.
17. Kim J, Park S, Jung Y, et al. Programmable real-time clinical photoacoustic and ultrasound imaging system. Sci Rep 2016;6(1):35137.
18. Li M, Liu C, Gong X, et al. Linear array-based real-time photoacoustic imaging system with a compact coaxial excitation handheld probe for noninvasive sentinel lymph node mapping. Biomed Opt Express 2018;9(4):1408–1422.
19. Ivankovic I, Razansky D. Non-invasive 3D imaging of the human carotid artery with volumetric multispectral optoacoustic tomography (vMSOT). Diagn Imaging Eur 2019;35(2):34–35. https://www.dieurope.com/site/wp-content/uploads/2019/05/DIEurope-AprilMay-2019.pdf. Accessed April 17, 2020.
20. Huang N, He M, Shi H, et al. Curved-array-based multispectral photoacoustic imaging of human finger joints. IEEE Trans Biomed Eng 2018;65(7):1452–1459.
21. Bohndiek SE, Bodapati S, Van De Sompel D, Kothapalli SR, Gambhir SS. Development and application of stable phantoms for the evaluation of photoacoustic imaging instruments. PLoS One 2013;8(9):e75533.
22. Toi M, Asao Y, Matsumoto Y, et al. Visualization of tumor-related blood vessels in human breast by photoacoustic imaging system with a hemispherical detector array. Sci Rep 2017;7:41970.
23. Deán-Ben XL, Razansky D. Functional optoacoustic human angiography with handheld video rate three dimensional scanner. Photoacoustics 2013;1(3-4):68–73.
24. Deán-Ben XL, Buehler A, Ntziachristos V, Razansky D. Accurate model-based reconstruction algorithm for three-dimensional optoacoustic tomography. IEEE Trans Med Imaging 2012;31(10):1922–1928.
25. Tzoumas S, Deliolanis N, Morscher S, Ntziachristos V. Unmixing molecular agents from absorbing tissue in multispectral optoacoustic tomography. IEEE Trans Med Imaging 2014;33(1):48–60.
26. Tzoumas S, Ntziachristos V. Spectral unmixing techniques for optoacoustic imaging of tissue pathophysiology. Philos Trans- Royal Soc, Math Phys Eng Sci 2017;375(2107):20170262.
27. Cox B, Laufer J, Beard P. The challenges for quantitative photoacoustic imaging. In: Oraevsky AA, Wang LV, eds. Proceedings of SPIE: photons plus ultrasound—imaging and sensing 2009. Vol. 7177. Bellingham, Wash: International Society for Optics and Photonics, 2009; 717713.
28. Chen Z, Deán-Ben XL, Liu N, et al. Concurrent fluorescence and volumetric optoacoustic tomography of nanoagent perfusion and bio-distribution in solid tumors. Biomed Opt Express 2019;10(10):5093–5102.
29. Zhang HF, Maslov K, Sivaramakrishnan M, Stoica G, Wang LV. Imaging of hemoglobin oxygen saturation variations in single vessels in vivo using photoacoustic microscopy. Appl Phys Lett 2007;90(5):053901.
30. Upputuri PK, Pramanik M. Recent advances in photoacoustic contrast agents for in vivo imaging. Wiley Interdiscip Rev Nanomed Nanobiotechnol 2020;12(4):e1618.
31. Siphanto RI, Thumma KK, Kolkman RG, et al. Serial noninvasive photoacoustic imaging of neovascularization in tumor angiogenesis. Opt Express 2005;13(1):89–95.
32. Rich LJ, Seshadri M. Photoacoustic imaging of vascular hemodynamics: validation with blood oxygenation level–dependent MR imaging. Radiology 2015;275(1):110–118.
33. Rich LJ, Miller A, Singh AK, Seshadri M. Photoacoustic imaging as an early biomarker of radio therapeutic efficacy in head and neck cancer. Theranostics 2018;8(8):2064–2078.
34. Solano F. Melanin and melanin-related polymers as materials with biomedical and biotechnological applications—cuttlefish ink and mussel foot proteins as inspired biomolecules. Int J Mol Sci 2017;18(7):1561.
35. Shao Q, Ashkenazi S. Photoacoustic lifetime imaging for direct in vivo tissue oxygen monitoring. J Biomed Opt 2015;20(3):036004.
36. Kim H, Chang JH. Multimodal photoacoustic imaging as a tool for sentinel lymph node identification and biopsy guidance. Biomed Eng Lett 2018;8(2):183–191.
37. Anani T, Brannen A, Panizzi P, Duin EC, David AE. Quantitative, real-time in vivo tracking of magnetic nanoparticles using multispectral optoacoustic tomography (MSOT) imaging. J Pharm Biomed Anal 2020;178:112951.
38. Shcherbakova DM, Verkhusha VV. Near-infrared fluorescent proteins for multicolor in vivo imaging. Nat Methods 2013;10(8):751–754.
39. Joseph J, Tomaszewski MR, Quiros-Gonzalez I, Weber J, Brunker J, Bohndiek SE. Evaluation of precision in optoacoustic tomography for preclinical imaging in living subjects. J Nucl Med 2017;58(5):807–814.

40. Luo S, Zhang E, Su Y, Cheng T, Shi C. A review of NIR dyes in cancer targeting and imaging. Biomaterials 2011;32(29):7127–7138.
41. Ilina K, MacCuaig WM, Laramie M, Jeouty JN, McNally LR, Henary M. Squaraine dyes: molecular design for different applications and remaining challenges. Bioconjug Chem 2020;31(2):194–213.
42. Zha Z, Deng Z, Li Y, et al. Biocompatible polypyrrole nanoparticles as a novel organic photoacoustic contrast agent for deep tissue imaging. Nanoscale 2013;5(10):4462–4467.
43. Li L, Liu T, Fu C, Tan L, Meng X, Liu H. Biodistribution, excretion, and toxicity of mesoporous silica nanoparticles after oral administration depend on their shape. Nanomedicine (Lond) 2015;11(8):1915–1924.
44. Zeiderman MR, Morgan DE, Christein JD, Grizzle WE, McMasters KM, McNally LR. Acidic pH-targeted chitosan capped mesoporous silica coated gold nanorods facilitate detection of pancreatic tumors via multispectral optoacoustic tomography. ACS Biomater Sci Eng 2016;2(7):1108–1120.
45. He YQ, Liu SP, Kong L, Liu ZF. A study on the sizes and concentrations of gold nanoparticles by spectra of absorption, resonance Rayleigh scattering and resonance non-linear scattering. Spectrochim Acta A Mol Biomol Spectrosc 2005;61(13-14):2861–2866.
46. Shrivastava R, Kushwaha P, Bhutia YC, Flora S. Oxidative stress following exposure to silver and gold nanoparticles in mice. Toxicol Ind Health 2016;32(8):1391–1404.
47. Hashem F, Nasr M, Ahmed Y. Preparation and evaluation of iron oxide nanoparticles for treatment of iron deficiency anemia. Int J Pharm Sci 2018;10(1):142.
48. Paramelle D, Sadovoy A, Gorelik S, Free P, Hobley J, Fernig DG. A rapid method to estimate the concentration of citrate capped silver nanoparticles from UV-visible light spectra. Analyst (Lond) 2014;139(19):4855–4861.
49. Cheng X, Zhong J, Meng J, et al. Characterization of multiwalled carbon nanotubes dispersing in water and association with biological effects. J Nanomater 2011;938491.
50. Pfohl M, Tune DD, Graf A, Zaumseil J, Krupke R, Flavel BS. Fitting single-walled carbon nanotube optical spectra. ACS Omega 2017;2(3):1163–1171.
51. Siegel RL, Miller KD, Jemal A. Cancer statistics, 2020. CA Cancer J Clin 2020;70(1):7–30.
52. Zografos G, Liakou P, Koulocheri D, et al. Differentiation of BIRADS-4 small breast lesions via multimodal ultrasound tomography. Eur Radiol 2015;25(2):410–418.
53. Berg WA, Gutierrez L, NessAiver MS, et al. Diagnostic accuracy of mammography, clinical examination, US, and MR imaging in preoperative assessment of breast cancer. Radiology 2004;233(3):830–849.
54. Leithner D, Wengert GJ, Helbich TH, et al. Clinical role of breast MRI now and going forward. Clin Radiol 2018;73(8):700–714.
55. Menke J. Photoacoustic breast tomography prototypes with reported human applications. Eur Radiol 2015;25(8):2205–2213.
56. Deán-Ben XL, Fehm TF, Gostic M, Razansky D. Volumetric hand-held optoacoustic angiography as a tool for real-time screening of dense breast. J Biophotonics 2016;9(3):253–259.
57. Abeyakoon O, Woitek RA, Wallis M, et al. Optoacoustic imaging increases the sensitivity of mammography and specificity of US: implications for practice [abstract]. Insights Imaging 2018;9(suppl 1):S415.
58. Neuschler EI, Butler R, Young CA, et al. A pivotal study of optoacoustic imaging to diagnose benign and malignant breast masses: a new evaluation tool for radiologists. Radiology 2018;287(2):398–412.
59. Kothapalli SR, Sonn GA, Choe JW, et al. Simultaneous transrectal ultrasound and photoacoustic human prostate imaging. Sci Transl Med 2019;11(507):eaav2169.
60. Peng K, He L, Wang B, Xiao J. Detection of cervical cancer based on photoacoustic imaging-the in-vitro results. Biomed Opt Express 2014;6(1):135–143.
61. Nandy S, Mostafa A, Hagemann IS, et al. Evaluation of ovarian cancer: initial application of coregistered photoacoustic tomography and US. Radiology 2018;289(3):740–747.
62. Qu Y, Li C, Shi J, et al. Transvaginal fast-scanning optical-resolution photoacoustic endoscopy. J Biomed Opt 2018;23(12):1–4.
63. Knieling F, Hartmann A, Claussen J, et al. Multispectral optoacoustic tomography in ulcerative colitis - a first-in-human diagnostic clinical trial. J Nucl Med 2017;58(supplement 1):1196. Accessed April 21, 2020. http://jnm.snmjournals.org/content/58/supplement_1/1196.
64. Schwarz M, Buehler A, Aguirre J, Ntziachristos V. Three-dimensional multispectral optoacoustic mesoscopy reveals melanin and blood oxygenation in human skin in vivo. J Biophotonics 2016;9(1-2):55–60.
65. Chuah SY, Attia AB, Long V, et al. Structural and functional 3D mapping of skin tumours with non-invasive multispectral optoacoustic tomography. Skin Res Technol 2017;23(2):221–226.
66. Roll W, Markwardt NA, Masthoff M, et al. Multispectral optoacoustic tomography of benign and malignant thyroid disorders: a pilot study. J Nucl Med 2019;60(10):1461–1466.
67. Krönke M, Karlas A, Fasoula N, et al. Multispectral optoacoustic tomography (MSOT): a novel label-free imaging technique for thyroid imaging. Nuklearmedizin 2019;58(02):142–143.
68. Masthoff M, Helfen A, Claussen J, et al. Multispectral optoacoustic tomography of systemic sclerosis. J Biophotonics 2018;11(11):e201800155.
69. Reber J, Willershäuser M, Karlas A, et al. Non-invasive measurement of brown fat metabolism based on optoacoustic imaging of hemoglobin gradients. Cell Metab 2018;27(3):689–701.e4.
70. Abeyakoon O, Morscher S, Dalhaus N, et al. Optoacoustic imaging detects hormone-related physiological changes of breast parenchyma. Ultraschall Med 2019;40(6):757–763.
71. Pan Z, Zhu L, Li Q, et al. Predicting initial margin status in breast cancer patients during breast-conserving surgery. OncoTargets Ther 2018;11:2627–2635.
72. Ha R, Friedlander LC, Hibshoosh H, et al. Optical coherence tomography: a novel imaging method for post-lumpectomy breast margin assessment—a multi-reader study. Acad Radiol 2018;25(3):279–287.
73. van de Ven SM, Elias SG, Chan CT, et al. Optical imaging with Her2-targeted affibody molecules can monitor hsp90 treatment response in a breast cancer xenograft mouse model. Clin Cancer Res 2012;18(4):1073–1081.
74. Dogan BE, Menezes GLG, Butler RS, et al. Optoacoustic imaging and gray-scale US features of breast cancers: correlation with molecular subtypes. Radiology 2019;292(3):564–572.
75. Fuchsjäger M, Shukla-Dave A, Akin O, Barentsz J, Hricak H. Prostate cancer imaging. Acta Radiol 2008;49(1):107–120.
76. Yang JM, Chen R, Favazza C, et al. A 2.5-mm diameter probe for photoacoustic and ultrasonic endoscopy. Opt Express 2012;20(21):23944–23953.
77. Lagergren J, Bergström R, Lindgren A, Nyrén O. Symptomatic gastroesophageal reflux as a risk factor for esophageal adenocarcinoma. N Engl J Med 1999;340(11):825–831.
78. Kolkman RG, Mulder MJ, Glade CP, Steenbergen W, van Leeuwen TG. Photoacoustic imaging of port-wine stains. Lasers Surg Med 2008;40(3):178–182.
79. Stoffels I, Jansen P, Petri M, et al. Assessment of nonradioactive multispectral optoacoustic tomographic imaging with conventional lymphoscintigraphic imaging for sentinel lymph node biopsy in melanoma. JAMA Netw Open 2019;2(8):e199020.
80. Oh JT, Li ML, Zhang HF, Maslov K, Stoica G, Wang LV. Three-dimensional imaging of skin melanoma in vivo by dual-wavelength photoacoustic microscopy. J Biomed Opt 2006;11(3):34032.
81. Dima A, Ntziachristos V. In-vivo handheld optoacoustic tomography of the human thyroid. Photoacoustics 2016;4(2):65–69.